UDK 621.376.32

Zh. T. Erdyneev, A. A. Geltser, E. P. Velikanova, N. V. Panokin

COMPARATIVE ANALYSIS OF FREQUENCY SCALING ALGORITHMS FOR SIGNAL PROCESSING IN SMALL-SIZE MOBILE PLATFORMS

Data of reciept 22.09.2017
Decision on publication 26.10.2017

Introduction. With the development of hardware and computer systems, which improve qualitative characteristics of synthetic aperture radars, with their dimensions limited, many new systems have appeared that allow using more accessible and widespread mobile platforms such as a car, quadcopters, unmanned aerial vehicles (UAV).

Problem. The use of new types of platforms leads to additional distortions associated with features of the geometry of the radar performance and more severe trajectory instabilities. Thus, new synthetic aperture radar systems should have special requirements for both software and hardware, which differ from classical systems.

Objective. The aim of the work is the comparison various algorithms that are used in modern radiovision systems to obtain high-quality radar images that can be integrated into various kinds of mobile platforms.

Methods. The method of frequency scaling and various modifications of this method are taken as a basic algorithm, including additional algorithms for compensating trajectory instabilities. For comparison of algorithms, the system geometry for automobiles and aircraft systems are considered and simulations were performed with the presence of point reflectors at different distances and the distortion of the platform motion.

Results. The difference of the considered algorithms in the form of flowcharts and mathematical formulas is shown. Based on results of the simulation the use of the basic frequency scaling algorithm at distances corresponding to the geometry of the automobile system leads to the distortion of the response along the azimuth. In addition, the use of the modified algorithm for compensating trajectory distortion allows correct focusing the targets at different distances.

Conclusion. The proposed combination of modified algorithms of trajectory distortion and frequency scaling allows focusing the image evenly throughout the frame and improving the quality of the image in the near zone.

Automobile, UAV, radiovision, radiolocation image (RLI), synthetic aperture radars (SAR), frequency modulated continuous wave (FMCW), frequency scaling algorithm (FSA).

The studies are being carried out with the financial support of the Ministry of Education and Science of the Russian Federation. Unique identification number of the Project RFMEFI57815X0130.

Introduction

With the development of hardware and computer systems, which improve qualitative characteristics of synthetic aperture radars (SAR) [1−7], with their dimensions limited, many new systems have appeared that allow using more accessible and widespread mobile platforms such as a car, quadcopters, unmanned aerial vehicles (UAV), in comparison with planes and satellites. The magnitude of the tasks which can be solved by means of these systems is enormous [8]. Cars would be able to generate panoramic radiolocation images (RLI) at the expense of their speed, using only one antenna system, which would decrease size requirements of the equipment [4, 5].

The new synthetic aperture radar systems should have special requirements for both software and hardware, which differ from classical systems. In the considered examples of the existing elaborations of algorithms and those ready for realisation in small-size SAR, one may point out the following [9−13]: the use of frequency modulated continuous wave (FMCW), algorithms for compensating trajectory distortions, and frequency scaling algorithm (FSA). The use of FMCW actually allows working in the near zone as well as decreases requirements for digital signal processing architecture [6], whereas among the frequency scaling methods [12, 13] there are different modifications, where different formulae are used. Consequently, in the article the following objectives have been set:

- to compare frequency scaling algorithm from the article [12] with the modified frequency scaling algorithm from the article [13] (hereinafter FSA-M);
- to apply the algorithm for compensating trajectory distortions from the article [12] for FSA and FSA-M and compare properties of the obtained radiolocation images;
- to compare properties of the radiolocation images at different slant ranges and azimuth position of point reflectors for detection of geometric distortions.

The article is arranged as follows. In the first part, the geometry of SAR performance is presented for the cases when UAV and cars are used as the bearing platforms. Their peculiarities and differences are demonstrated as well. In the second part, the processing algorithms of FSA and FSA-M are briefly discussed. In the third part, the results of processing of signals are shown, which are obtained during simulation of SAR performance by virtue of different methods of compression and compensation of radiolocation image. In the end of the article, the conclusion is given.

1. The geometry of SAR performance

First of all, it is necessary to set the source conditions, therefore let us consider the principle and geometry of the synthetic-aperture radar performance, derive formula, corresponding to the received signal after its multiplying by reference signal.

Let us suppose, that the sounding signal $s_t(t)$ radiates in the moment of time τ at which the distance is $R(\tau)$ and returns to the receiver in the moment of time $\tau + \tau_d$, covering the distance $R(\tau + \tau_d)$. Thus, the delay of signal double scattering may be expressed as:

$$\tau_d = \frac{R(\tau) + R(\tau + \tau_d)}{c}, \tag{1}$$

where $R(\tau + \tau_d) = \sqrt{R_0^2 + v^2 \cdot (\tau + \tau_d - \tau_0)^2}$;

c – the speed of light;

v – the velocity of the moving platform.

Simplifying the formula (1) by quadratic equation, confining ourselves to quadratic terms of expansion, we obtain the following formula of the delay value:

$$\tau_d(\tau) = \frac{2\left(\frac{R(\tau)}{c} + \frac{v^2}{c^2}(\tau - \tau_0)\right)}{1 - \frac{v^2}{c^2}}. \tag{2}$$

Considering the formula (2) and the use of the linear frequency modulation signal, the received signal may be expressed as follows:

$$s_r(t, \tau) = \sigma(\tau_0, r_0) \cdot s_t\left(t - \tau_d(\tau)\right) \cdot \exp\left[j2\pi f_0 \left(t - \tau_d(\tau)\right)\right],$$

where $\sigma(\tau_0, r_0)$ – target cross-section with the corresponding coordinates;

f_0 – carrier wave frequency;

$s_t(t) = \exp(j\pi K_r t^2)$ – linear frequency modulation signal, where K_r – frequency slew rate, which is calculated as $\Delta F / T$, where ΔF – signal band;

T – period of one pulse (period of pulse radiation).

For the cases when FMCW is used, the received signal is multiplied by reference complex conjugate signal:

$$s_{ref}(t) = s_t^*(t) \cdot \exp(-j2\pi f_0 t).$$

After multiplying by reference complex conjugate signal we obtain the following signal:

$$\begin{aligned} s_b(t,\tau) &= \sigma(\tau_0, r_0) \cdot \exp\left[-j2\pi K_r \tau_d(\tau) \cdot t\right] \times \\ &\times \exp\left[-j2\pi f_0 \tau_d(\tau)\right] \cdot \exp\left[-j2\pi K_r \tau_d^2(\tau)\right]. \end{aligned} \quad (3)$$

Let us analyse the formula (3) in detail. The first exponent forms harmonic signal with the frequency corresponding to multiplication of delay $\tau_d(\tau)$ and the frequency slew rate K_r, and thus, it is responsible for *the location of the target by range*. The second exponent forms the Doppler spectrum along the azimuth making it possible to determine *the location of the target by azimuth*. The third exponent is called residual video phase and is compensated in most cases due to its uselessness [14].

Let us analyse the difference between UAV and an automobile used as platforms for aperture synthesis. To illustrate the difference in the geometry of SAR on automobile and aircraft platforms, the fig. 1 is given below. Let us assume that antenna system parameters and the height of the aircraft platform make the following values, given in the table 1.

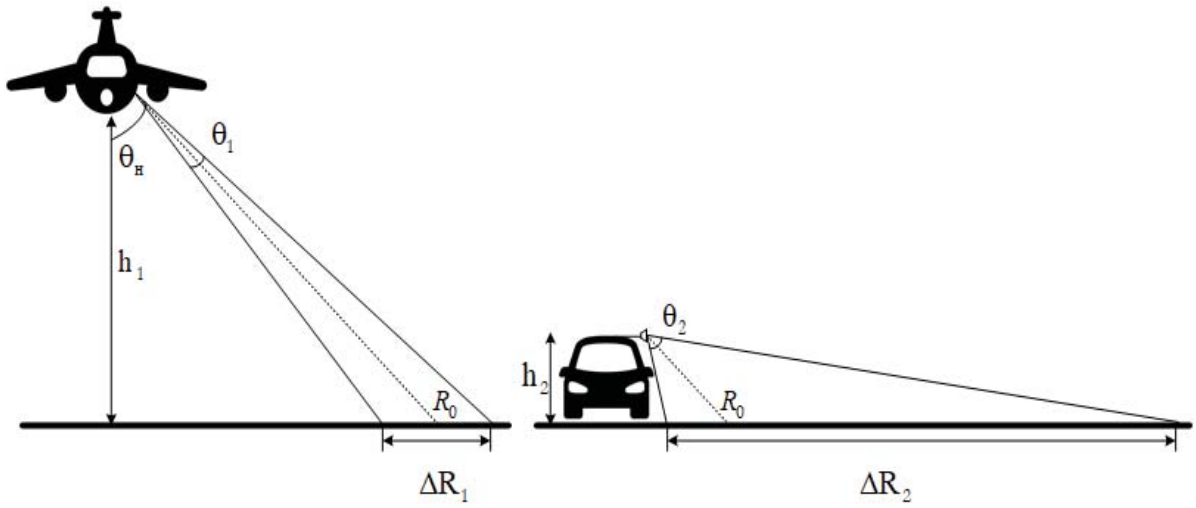

Fig. 1. The geometry of SAR on automobile and aircraft platforms

Table 1

Parameters of the geometry of aircraft and automobile SAR

Parameter	Value
Antenna system look angle, $\theta_н$, degrees	45°
Width of directional diagram by azimuth, θ, degrees	15°
Width of directional diagram by elevation, θ_1, degrees	15°
Height of the aircraft platform, h_1, m	1000
Height of the automobile platform, h_2, m	2

Now, if we calculate the swath width along the range via antenna system look angle and width of directional diagram by elevation, we obtain:

$$\Delta R_1 = \left(h_1 / \cos(\theta_н + \theta_1 / 2)\right) - \left(h_1 / \cos(\theta_н - \theta_1 / 2)\right) = 382 \text{ м.}$$

If we calculate the length of aperture synthesis by the formula:

$$L_s = 2 \cdot R_0 \cdot \tan(\theta / 2) = 372 \text{ м.}$$

As it may be seen, the sizes of zones in both coordinates are commensurate, which is convenient for displaying the final radiolocation image. If the parameters of the antenna system remain the same, with the antenna system placed on the automobile platform of 2 metres high ($h_2 = 2$ m), the width of the look will be: $\Delta R_2 = 0{,}76$ м. As a result, in the final image the size of the image in terms of range will be only 0,76 metres, which is absolutely impractical for this system.

Therefore, it is advisable to use an antenna system with a broader directional diagram by elevation when the automobile platform is used or any other platform requiring low height of antenna synthesis. For instance, if we now take an antenna with the directional diagram width by elevation $\theta_2 = 80°$, then $\Delta R_2 = 21$ м. In some cases the antenna system is installed higher by virtue of additional fastenings, as it may be seen from [5, 7], which is not surprising when it comes to receiving data from remote zones.

Now that we have formed the mathematical model of the received signal and the geometry of the performance, let us carry out simulation of the SAR performance and data processing by FSA and FSA-M algorithms with a point reflector for comparison of the following parameters:

- the azimuth and range resolution;
- the relation of the side lobes' level to the main lobe one;
- integral relation of side lobes' level to that of the main one.

2. Processing algorithms

As it was previously mentioned, let us take two realisation of FSA algorithms for processing algorithms. Their flowcharts are given in the fig. 2 [12, 13].

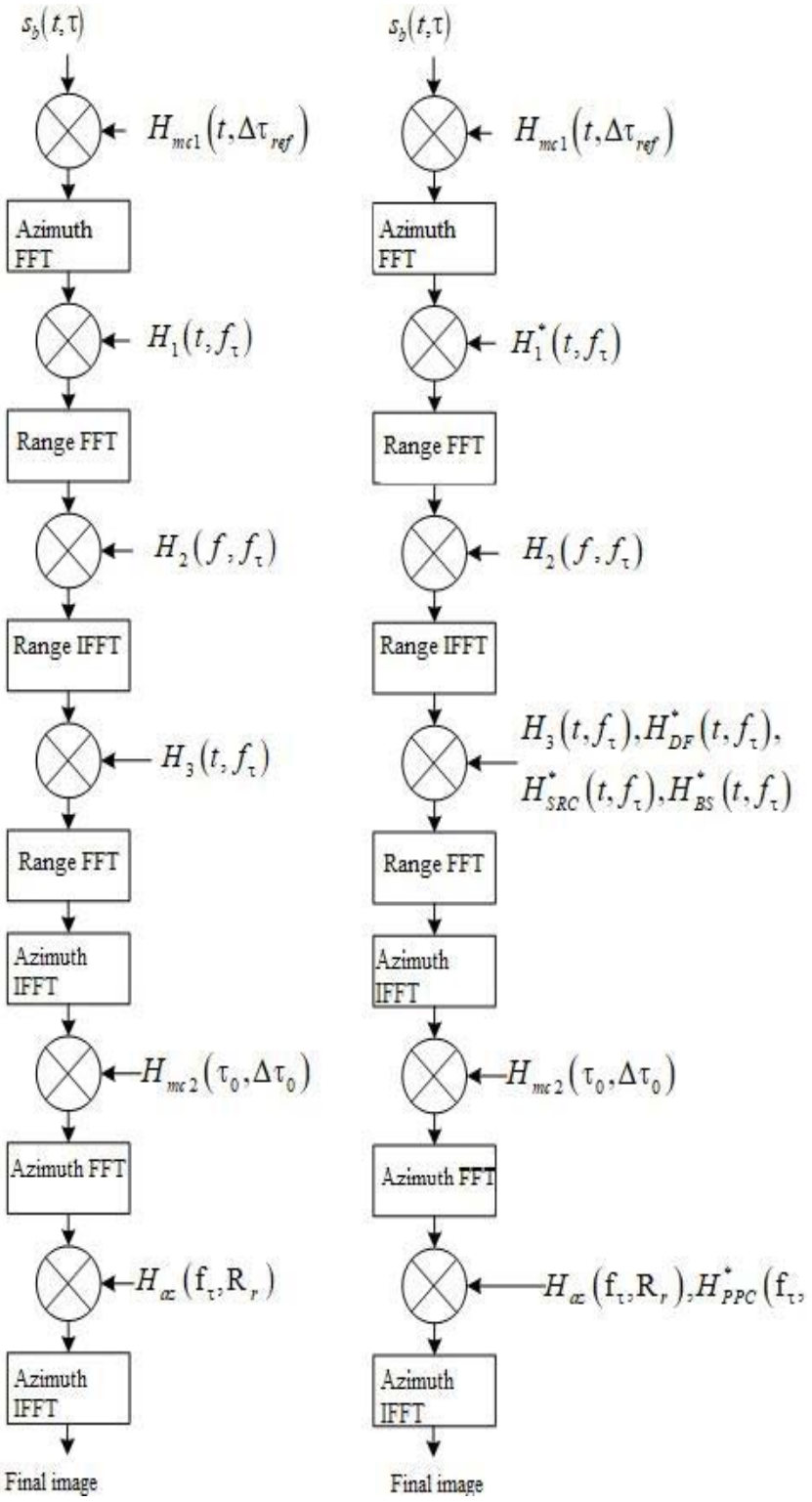

Fig. 2. Flowcharts of FSA (left) and FSA-M (right)

It needs to pointed out straightaway that the full information about processing stages is given in the sources [12, 13]. Below, the formulae used either for one modification or for trajectory instabilities compensations, will be given. The trajectory instability has also been considered within only one modification.

The main feature of frequency scaling algorithms consists in the range migration for different targets may be compensated without interpolation, only by mere multiplication. This advantage makes this algorithm more attractive for integration into signal processing block, since multiplication operations are simpler than interpolation ones.

The input data of the algorithm are the array of signals from the output of the multiplier, according to the formula (3).

The FSA algorithm includes a series of Fast Fourier Transformation (FFT) and phase multiplications. If we reject the stages of compensation of the platform movement, the key differences between the algorithms will be:

Frequency scaling function for FSA, which removes Doppler oscillations, has the following view:

$$H_1(t,\ f_\tau) = \exp\left(-j\cdot\left(2\pi\cdot f_\tau\cdot t + \pi\cdot K_r\cdot t^2\left(1-D(f_\tau, v)\right)\right)\right),$$

where $D(f_\tau, v) = \sqrt{1-\lambda^2\cdot f_\tau^2/4v^2}$;

λ – wavelength;

f_τ – azimuth grid frequency.

The formula for the modified FSA-M algorithm is of the following view:

$$H_1^*(t,\ f_\tau) = \exp\left(-j\cdot\pi\cdot K_r\cdot t^2\left(1-D(f_\tau, v)\right)\right).$$

In the modified algorithm after Inverse Fast Fourier Transformation (IFFT), the multiplication by three more functions takes place:

1) doppler factor correlation function:

$$H_{DFC}^*(t,\ f_\tau) = \exp\left(-j\cdot 2\pi\cdot f_\tau\cdot D(f_\tau, v)\cdot t\right);$$

2) second range compression function:

$$H_{SRC}^*(t, f_\tau) =$$

$$= \exp\left(-j\frac{2\pi\cdot R_{ref}\cdot K_r^2\cdot\lambda}{c^2}\cdot\frac{\left(D^2(f_\tau, v)-1\right)}{D^3(f_\tau, v)}\cdot\left(D(f_\tau, v)\cdot t-\frac{2\cdot R_{ref}}{c}\right)^2\right)\bullet$$

$$\exp\left(-j\frac{2\pi \cdot R_{ref} \cdot K_r^3 \cdot \lambda^3}{c^3} \cdot \frac{\left(D^2(f_\tau, v)-1\right)}{D^5(f_\tau, v)} \cdot \left(D(f_\tau, v)\cdot t - \frac{2\cdot R_{ref}}{c} \right)^3 \right);$$

3) group phase shift function:

$$H^*_{BS}(t,\ f_\tau) =$$

$$= \exp\left(j\cdot\frac{4\pi\cdot K_r}{c}\cdot R_{ref}\cdot\left(\frac{1}{D(f_\tau, v)}-1\right)\left(D(f_\tau, v)\cdot t - \frac{2\cdot R_{ref}}{c} \right)\right),$$

where R_{ref} – reference range.

At the final the multiplication by phase conservation phase:

$$H^*_{PPC}(f_\tau,\ f_r) = \exp\left(j\frac{4\pi\cdot R_{ref}}{c}\frac{f_r}{D(f_\tau, v)} \right),$$

where f_r – range frequency grid.

Let us analyse the peculiarities of the radar movement itself. The algorithms mentioned above took into account only even, direct movement. Actually, the platform will often deviate from its nominal trajectory, which will result in poor radiolocation image quality.

On the basis of [12, 15], the following algorithm of movement compensation is suggested. The receive signal $s_b(t,\tau)$ is multiplied by the function:

$$H_{mc1}(t, \Delta\tau_{ref}) = \exp\left(-j\begin{pmatrix} \omega_0\cdot\Delta\tau_{ref} + 2\pi\cdot K_r\cdot t\cdot\Delta\tau_{ref} - \\ -\pi\cdot K_r\cdot(2\cdot\tau_{ref}\cdot\Delta\tau_{ref} - \Delta\tau^2_{ref}) \end{pmatrix}\right), \qquad (4)$$

where $\Delta\tau_{ref} = 2\cdot\Delta R_{ref}/c$; $\Delta R_{ref} = R_{actual} - R_{ideal}$, where R_{actual} – slant range from platform to point target considering known deviations during platform movement;

R_{ideal} – ideal trajectory of platform movement for the same location of the point target.

The next stage carries out differential correction after range compensation, where the location information is averaged along the entire pulse. This statement comes out of the fact that when all data are compressed by range, each cell in

range is formed from data that is distributed along the entire pulse. Correction function is calculated for each cell by range:

$$H_{mc2}(\tau_r, \Delta\tau_r) = \\ = \exp\left(j\left(\begin{array}{l} -\omega_0 \cdot \Delta\tau_r + 2\pi \cdot K_r \cdot \tau_r \cdot \Delta\tau_r - \pi \cdot K_r \cdot \Delta\tau_0^2 + \\ +\omega_0 \cdot \Delta\tau_r - 2\pi \cdot K_r \cdot \tau_r \cdot \Delta\tau_r + \pi \cdot K_r \cdot \Delta\tau_{ref}^2 \end{array} \right) \right). \quad (5)$$

The introduced method is similar to traditional movement compensation, but has a number of advantages. Firstly, the movement during radiation is taken into account, which is crucial for modulation with continuous chirp. Secondly, the correction here takes place without interpolation.

Now, let us carry out imitation modelling with the parameters given in the table 2.

Table 2

Modelling parameters

Parameter	Value
Type of signal modulation	chirp
Platform velocity	100 km/h
Carrier wave frequency	10 GHz
Period of pulse	1 ms
Modification strip of chirp	50 MHz
Targets' coordinates, [range, m; azimuth, m]	[650, 0], [20; 0], [300; 0], [100; 0]

Let us compare the algorithms with different modifications in the following sequence:

1) radiolocation image of the target at the range of 650 metres, obtained by methods FSA and FSA-M with an ideal trajectory correction;

2) radiolocation image of the target at the range of 20 metres, obtained by FSA and FSA-M methods with an ideal trajectory correction;

3) radiolocation image of two targets at the range of 100 metres and 300 metres with a rough trajectory correction, where 100 metres is reference range;

4) radiolocation image of two targets at the range of 100 metres and 300 metres obtained by means of FSA and FSA-M methods, with a proposed trajectory, where 100 metres is reference range.

3. Modelling. Processing results

The results of the modelling of the first two points are shown in the fig. 3–6 and the table 3.

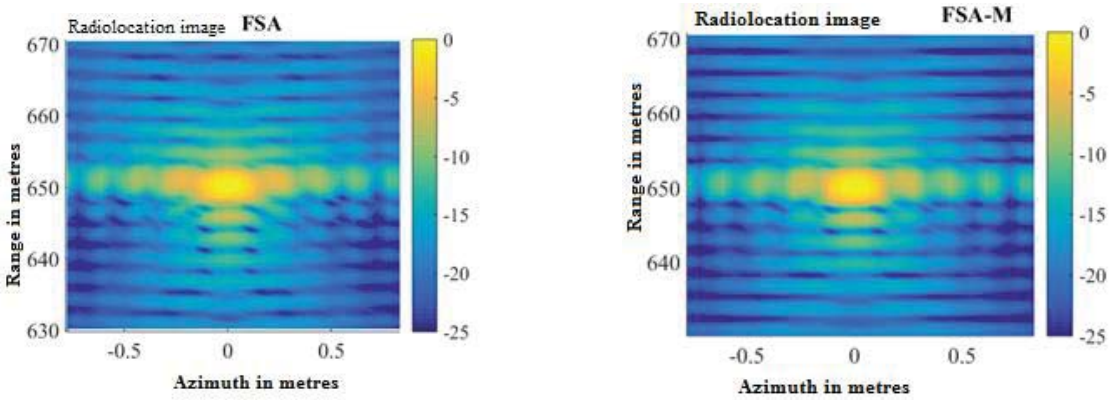

Fig. 3. Radiolocation image of the point target obtained by FSA (left) and FSA-M (right) methods at the range of 650 metres

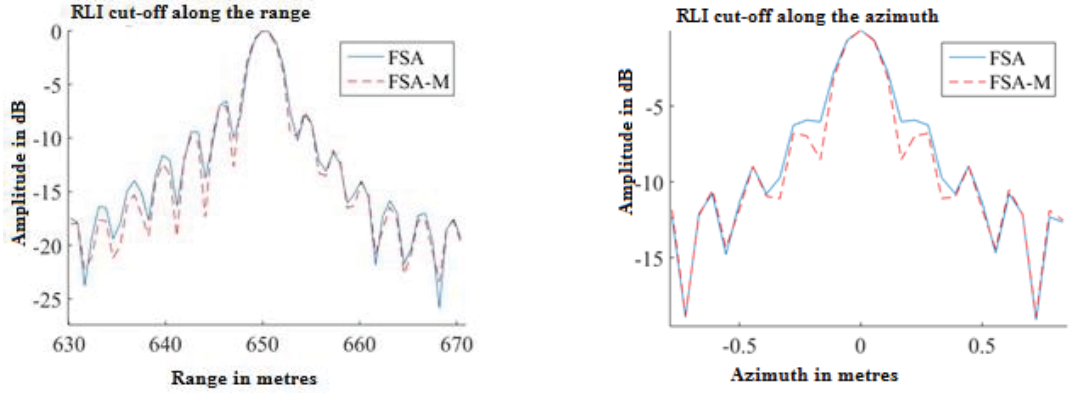

Fig. 4. Point target RLI cut-offs (650 m range) along the range (left) and azimuth (right) for FSA and FSA-M methods

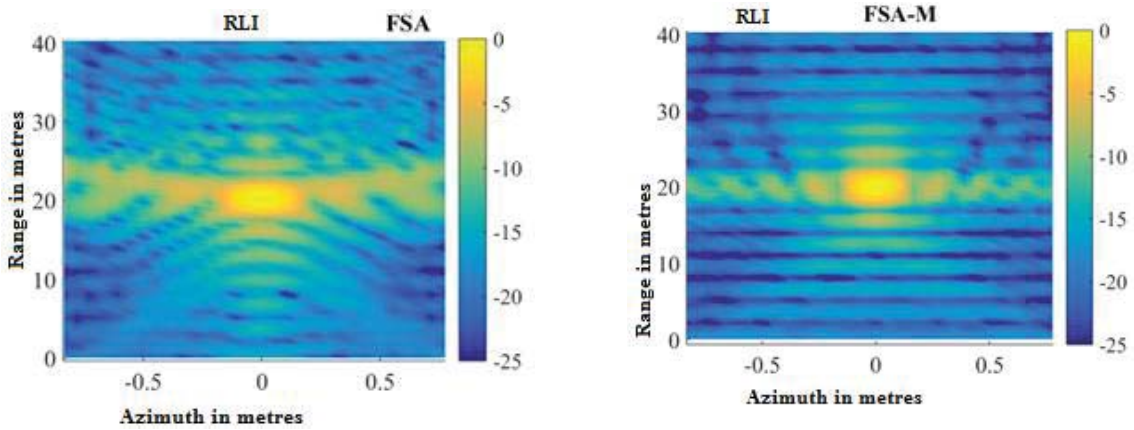

Fig. 5. Radiolocation image of the point target obtained by FSA (left) and FSA-M (right) methods at the range of 20 metres

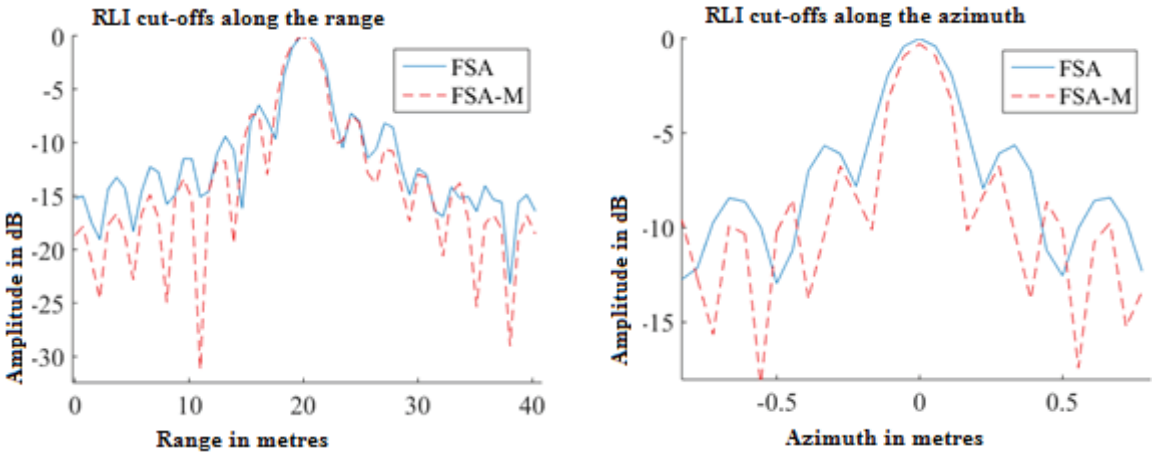

Fig. 6. Point target RLI cut-offs (20 m range) along the range (left) and the azimuth (right) for FSA and FSA-M methods

Table 3

RLI properties obtained by virtue of FSA and FSA-M methods during imitation modelling of targets at the range of 650 metres and 20 metres

Parameter	FSA	FSA-M	FSA	FSA-M
Range, m	650		20	
Range resolution	3,6	3,58	3,5	3,6
Azimuth resolution	0,23	0,22	0,27	0,21
Range side lobes' level	–7,2	–7,2	–7	–7,4
Azimuth side lobes' level	–5,9	–6,8	–5,7	–6,9
Integral range side lobes' level	5,1	5,5	4	5,6
Integral azimuth side lobes' level	1,4	1,6	1	1,5

During analysis of the trajectory instability, a sinusoidal distortion was detected during motion of platform along the range. It is shown in the fig. 7. Consequently, in each *i*-th pulse the phase shift will take place corresponding to the value $\exp(-j \cdot 4 \cdot pi \cdot R(i)/\lambda)$. On the assumption that the trajectory is known, let us compare to approaches for elimination of phase distortions. The first case is a classical one for which the formula (4) is used, whereas the formulae (4) and (5) are used for the second one. It needs pointing out that 100 metres value has been taken as a reference range. In the fig. 8–11 and in the tables 4, 5 the results of the modelling are given.

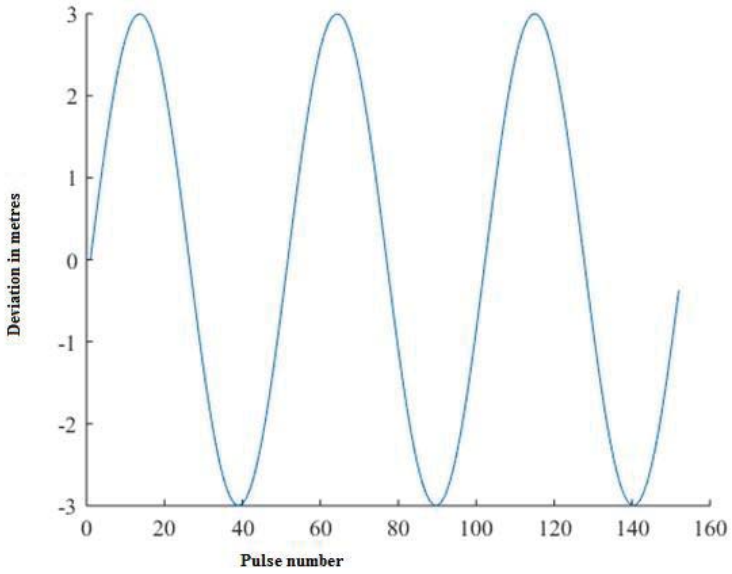

Fig. 7. Trajectory instability of the platform

a

b

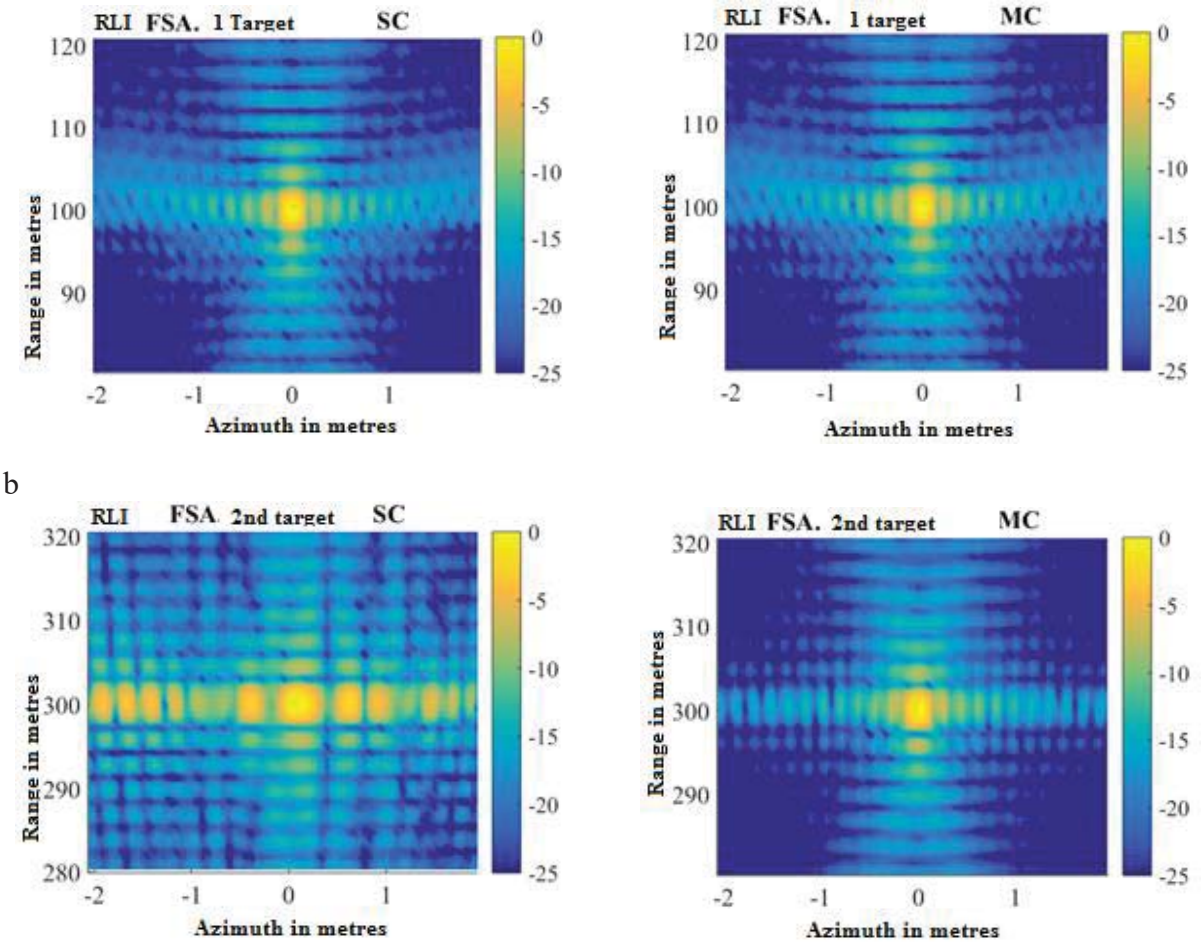

Fig. 8. Radiolocation images of point targets obtained by FSA method, at the range of 100 m (a), 300 m (b), and obtained by classical method (left) and modified method (right) of trajectory deviation compensation

a

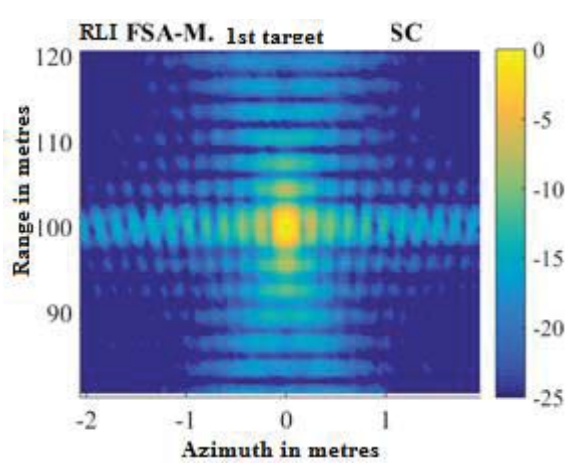

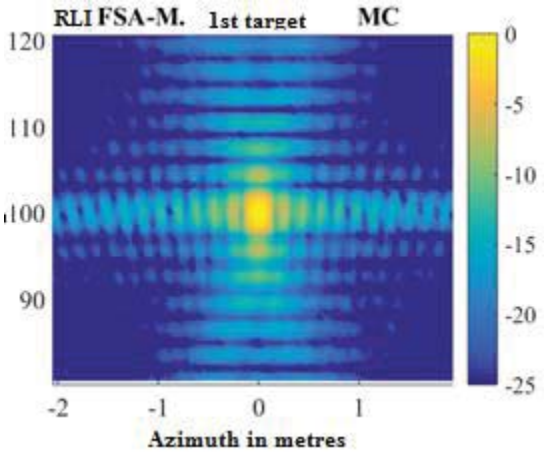

b

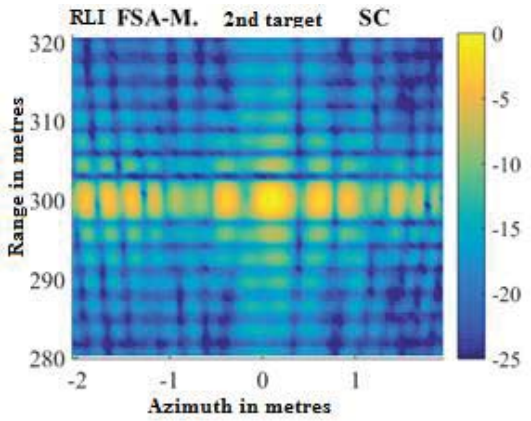

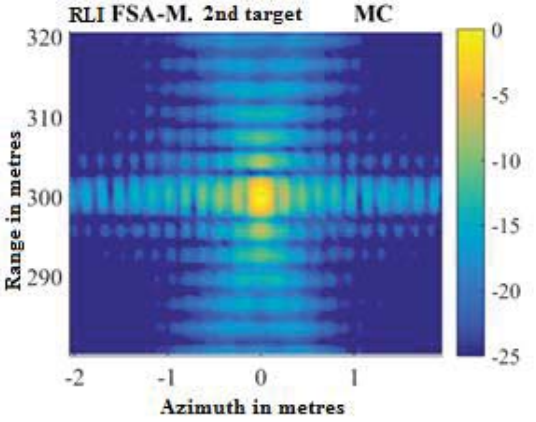

Fig. 9. Radiolocation images of point targets obtained by FSA-M method, at the range of 100 m (a), 300 m (b), and obtained by classical method (left) and modified method (right) of trajectory deviation compensation

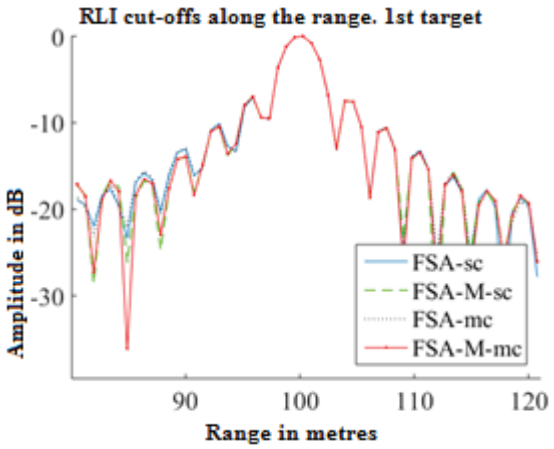

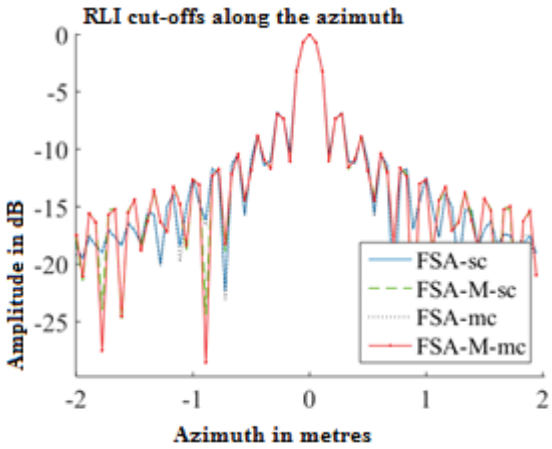

Fig. 10. Point target RLI cut-offs (100 m range) obtained by FSA and FSA-M methods along the range (left) and along the azimuth (right) for classical method (SC) and for modified method (MC) of trajectory distortion compensation

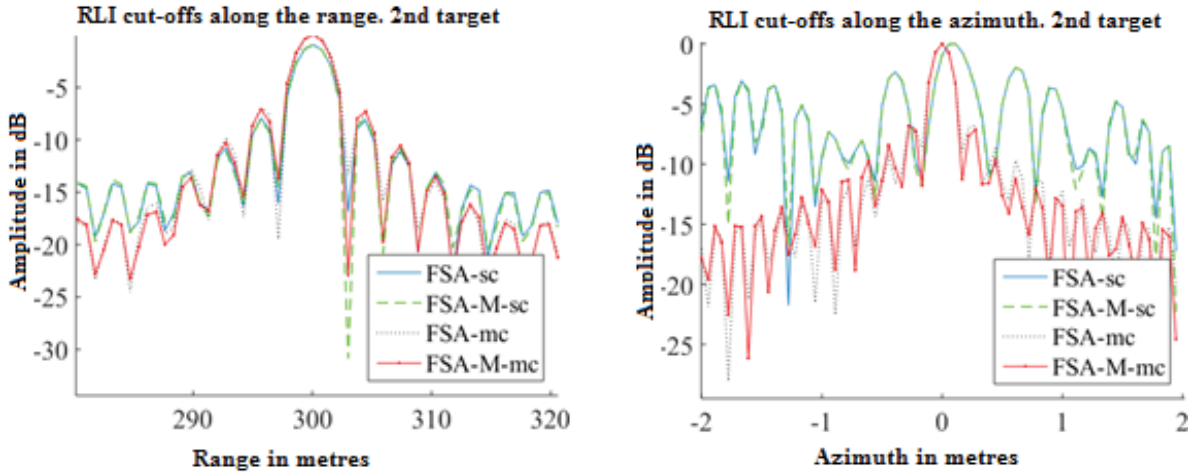

Fig. 11. Point target RLI cut-offs (300 m range) obtained by FSA and FSA-M methods along the range (left) and along the azimuth (right) for classical method (SC) and for modified method (MC) of trajectory distortion compensation

Table 4

Properties of RLI obtained by FSA methods during modelling for point targets with classical and modified methods of trajectory distortion compensation

Parameters	Classical compensation		Modified compensation	
Number of target	1st target	2nd target	1st target	2nd target
Range coordinates of targets, m	100	300	100	300
Range resolution	3,6	3,62	3,6	3,65
Azimuth resolution	0,22	0,3	0,21	0.21
Range side lobes' level	–7,3	–6,9	–7,3	–7,2
Azimuth side lobes' level	–6,8	–2,1	–6,8	–6,8
Integral range side lobes' level	3,5	–9,7	3,5	–16,2
Integral azimuth side lobes' level	1,35	0,03	1,32	1,6

Table 5

Properties of RLI obtained by FSA-M methods during modelling for point targets with classical and modified methods of trajectory distortion compensation

Parameters	Classical compensation		Modified compensation	
Number of target	1st target	2nd target	1st target	2nd target
Range coordinates of targets	100 м	300 м	100 м	300 м
Range resolution	3,58	3,64	3,6	3,6
Azimuth resolution	0,21	0,31	0,21	0,21
Range side lobes' level	–7,3	–6,8	–7,25	–7,2
Azimuth side lobes' level	–6,9	–2,1	–6,9	–7
Integral range side lobes' level	3,6	11,4	3,6	–15
Integral azimuth side lobes' level	1,32	–0,27	1,3	1,7

The results of the studies enable the following conclusions.

The use of FSA algorithm on ranges corresponding to the geometry of the automobile system performance leads to smearing the response of the point target basically along the azimuth surface. If we compare the results, obtained by virtue of FSA-M algorithm, where the image was more sharp, the azimuth resolution improved by 23 %, the azimuth side lobes' level was lower by 1,2 dB. The level of integral side lobes on both axis became bigger at FSA-M, but this is connected with decrease of the resolution. As for the range, there are also some alterations, but they are not that significant. The geometry of aircraft performance also demonstrates improvements when the modified FSA algorithm is in use.

The application of the modified trajectory distortion compensation, in comparison with the traditional one, enables focusing the target correctly, which are in different planes, as it is shown in the fig. 11. Numerically, integral side lobes in case of the modified one application for 2^{nd} target becomes better by 6,5 dB at FSA and 26,4 dB at FSA-M. The common level of integral side lobes in the modified case for both FSA and FSA-M differs by 1,2 dB. The improvement of resolution is also observed.

Conclusion

According to the results of the work conducted, the imitation modelling of two algorithms FSA (traditional and modified) was carried out, for signal processing of SAR. Also their comparative analysis was carried out on the subject of resolution, integral level of side lobes and level of side lobes. The results of the modelling gives us the opportunity to obtain a more detailed and sharp image irrespective of the geometry of the system performance and choice of reference range while eliminating trajectory distortions. Therefor it will be suitable for application on any platforms.

References

1. González-Partida J.T., Almorox-Gonzalez P., Burgos-Garcia M. Dorta-Naranjo B.P. *Sensors*, 2008, T. 8, no. 5, pp. 3384–3405.

2. Chang W., Tian H., Gu C. FMCW SAR: From design to realization, Geoscience and Remote Sensing Symposium (IGARSS), Beijing, China, *IEEE Int*., 2016, pp.1122–1125.

3. Chang W., Tian H., Li X. Miniature high resolution FMCW SAR system, Modern Circuits and Systems Technologies (MOCAST), *5th Int. Conf. IEEE*, Thessaloniki, Greece, 2016, pp. 1–4.

4. Luo Y., Hongjun S., Wang R., Shichao Z. *J. Electron*. (*China*), 2013, T. 30, no. 6, pp. 561–566.

5. Cho B.L., Kong Y.K., Park H.G., Kim Y.S. *IEEE Geosci. Remote Sens. Lett*., 2006, T. 3, no. 3, pp. 401–405.

6. Meta A. Signal processing of FMCW synthetic aperture radar data. PhD thesis, TU Delft, Delft Univ. Technol., 2006.

7. Gromek D., Krysik P., Ndini K., Samczynski P. FMCW SAR based on USRP hardware platform, *Radar Conf. IEEE*, 2014, Cincinnati, OH, USA, 2014, pp. 0552–0555.

8. Ouchi K. *Remote Sensing*, 2013, T. 5, no. 2, pp. 716–807.

9. Lort Cuenca M. Ground-based SAR imaging basics and land clutter effects on the focused image: PhD thesis. Univ. Politècnica de Catalunya, 2014.

10. De Wit J.J.M. Development of an Airborne Ka-band FMCW Synthetic Aperture Radar, PhD thesis, TU Delft, Delft Univ. Technol., 2005.

11. Stringham C. Developments in LFM-CW SAR for UAV Operation, PhD thesis, Brigham Young Univ., 2014.

12. Zaugg E.C., Long D.G., *IEEE Trans. Geosci. Remote sensing*, 2008, T. 46, no. 10, pp. 2990–2998.

13. Jiang Z. Huang F., Wan J., Cheng Z. *Chin. J. Aeronaut*., 2007, T. 20, no. 4, pp. 339–345.

14. Carrara W.G., Goodman R.S., Majewski R.M. Spotlight Synthetic Aperture Radar Signal Processing Algorithms. Boston, MA, Artech House, 1995.

15. Fornaro G. *IEEE Trans. Aerosp. Electron. Syst*., 1999, vol. 35, no. 3, pp. 997–1009.

Information about the authors:
Zhargal T. ERDYNEEV, Post-graduate student.
E-mail: erdineevzh@gmail.com
Andrey A. GELTSER, Cand. sci. (End.), chair.
E-mail: gaa.pochta@gmail.com
Elena P. VELIKANOVA, Cand. sci. (Eng.), Associate Prof.
E-mail: Raliens@mail.ru
Tomsk State University of Control Systems and Radioelectronics
Nikolay V. PANOKIN, Cand. sci. (Eng.)
Direktorat Head of science.
E-mail: n.panokin@misis.ru
National University of Science and Technology «MISIS»